IEEE Access
Multidisciplinary | Rapid Review | Open Access Journal

Received September 27, 2020, accepted October 12, 2020, date of publication October 15, 2020, date of current version October 29, 2020.

Digital Object Identifier 10.1109/ACCESS.2020.3031370

Improving External Quantum Efficiency by Subwavelength Nano Multi-Layered Structures for Optoelectronic Devices

DONG WANG[1,3], RUI ZHOU[2,4], YINGHUI WU[1,3], HOUZHI CAI[1,3], AND YUEQIANG ZHANG[1,3]

[1]Key Laboratory of Optoelectronic Devices and Systems of Ministry of Education and Guangdong Province, Shenzhen University, Shenzhen 518060, China
[2]Waytous Inc., Beijing 100000, China
[3]College of Physics and Optoelectronic Engineering, Shenzhen University, Shenzhen 518060, China
[4]Qingdao Academy of Intelligent Industries, Qingdao 266000, China

Corresponding author: Yueqiang Zhang (yueqiang.zhang@szu.edu.cn)

This work was supported in part by the National Natural Science Foundation of China (NSFC) under Grant 11775147, in part by the Guangdong Basic and Applied Basic Research Foundation under Grant 2019A1515011474 and Grant 2019A1515110130, and in part by the Science and Technology Program of Shenzhen under Grant JCYJ20180305125443569 and Grant JCYJ20190808115605501.

ABSTRACT Based on thin film optics (TFO) and finite element method (FEM), we have theoretically investigated improving external quantum efficiency (EQE) by anti-reflection (AR) films constructed from subwavelength nano multi-layers (NML) of low and high index materials, where the low and high index materials are MgF_2 and Ta_2O_5, respectively. This kind of NML dielectric structures have the advantages of low-cost and flexible. Three kinds of substrates have been studied here, which are glass, polyethylene naphthalate (PEN), and polyethylene terephthalate (PET), respectively. TFO theory has been used to obtain the transmittance and reflectance, which agrees well with FEM results. For NML structure, TFO is more efficient than FEM in terms of calculation time and accuracy. The average AR effects (AAREs) are about 3.69%, 3.46% and 3.07% on glass substrate, about 6.15%, 5.56% and 5.02% on PEN substrate, and about 5.06%, 4.62% and 4.17% on PET substrate, for AR bands (ARBs) 350∼800 nm, 350∼1100 nm and 350∼1500 nm, respectively. The results also reflect that wider AR bandwidth needs more NML layers. In practice, this kind of AR films can be widely applicable to enhance the EQE of the optoelectronic devices (OEDs).

INDEX TERMS Anti-reflection, nano multi-layers, thin film optics, finite element method.

I. INTRODUCTION

Transparent conductive substrates (TCSs) are characterized by their high transmission of visible light and simultaneously very high electrical DC (direct current) sheet conductivity [1]–[6]. TCSs can be applied as the transparent electrodes, which are the key component of optoelectronic devices (OEDs) for information (displays) and energy (photovoltaics, window glass and architectural) technologies [7]–[9]. External quantum efficiency (EQE) is an important physical quantity to evaluate the performance of OEDs. Besides optimizing the electronic characteristics of each structure of OEDs and reducing the recombination of electrons and holes, EQE also takes into account the optical performance of the device, which contains transmissivity, absorptivity and reflectivity. Introducing optical methods and applying anti-reflection (AR) layer is an important way to improve optical performance and then enhance EQE of the OEDs. Generally, nanoscale periodic structures are adopted to achieve AR layer in most works [10]–[12]. However, such nanoscale periodic structures are manufactured skillfully by costly techniques such as lithography and nano-imprint lithography. Therefore, high efficiency and low-cost AR layers are very meaningful for OEDs in both academia and industry.

One-dimensional Bragg photonic crystals (BPCs) with the Bragg back reflector structures has been used in OEDs to reduce the reflection of incident light [13]–[15]. BPCs are characterized by periodic medium structures with photonic band gap (PBG), which can control the path of light [16], [17]. PBG can be obtained by electromagnetic simulation on a determined PBC. The electromagnetic simulation methods generally include FDTD (finite difference time domain) and FEM (finite element method) [18], [19]. However, these

The associate editor coordinating the review of this manuscript and approving it for publication was Kin Kee Chow.

simulation methods (FDTD and FEM) are time-consuming, especially for the case that the structure size is much smaller than the wave length.

In this article, the theory of thin film optics (TFO) [20] is applied to study one-dimensional BPC, which is characterized as nano multi-layers (NML). It is worth noting that simulation based on TFO takes much less time than FDTD and FEM. Therefore, it is easier to design the corresponding BPC structure from the desired PBG structure by TFO. Finally, FEM has also been used as a contrast to simulate the NML, and the results were consistent with TFO theory. However, for NML structure TFO is more efficient than FEM in terms of calculation time and accuracy. For FEM, the more accurate the result is, the denser the mesh is, resulting in a longer computation time.

This kind of NML AR film can be fabricated by low-cost techniques, for example magnetron sputtering, electron beam evaporation, and thermal deposition process. Commercial software based on TFO is widely used to guide the industrial production of optical film, such as optical film design of lenses. TFO can also be used to guide the research activities of design, analysis, and monitoring of optical film coatings [1], [21]–[24].

We have studied the NML AR films of TiO_2 and SiO_2 in the early work [25], where two grades AR films have been investigated. The 1-st NML AR films involve the interface of substrate and air, and the 2-nd NML AR films involve the interface of transparent conductive film and substrate. In Ref. [25], the AR effect of the 2-nd AR is much smaller than the 1-st AR. In view of the practical fabrication of OEDs only affecting the 2-nd AR, we will focus on the need for the NML AR film of MgF_2 and Ta_2O_5 at the interface between substrate and air. It is worth noting that the previous work concentrates on the AR ability of a specific band range. However, this article concentrates on the possibility of the AR band extension to different bandwidths. In addition, FEM is used as a contrast. Finally, it reflects that wider AR bandwidth means more NML layers, and TFO is more efficient than FEM in terms of calculation time and accuracy. There are previous published works also about using MgF_2 and Ta_2O_5 NML as AR coating [26,27]. Their NML AR films are much more than 30 layers and obey some periodic rules. Our NML films break the periodic rules, and are only dozen layers or less with better AR effect.

II. PRINCIPLE

Generally, OEDs structure is based on TCSs, such as FTO (fluorine-doped tin oxide) glass, ITO (indium tin oxide) glass, FTO PEN (polyethylene naphthalate) plastic, ITO PEN, FTO PET (polyethylene terephthalate), ITO PET, and so on [1]–[9], [25]. TCS is constructed of substrate and transparent conductive film. As shown in Fig. 1, our NML AR film is on the outside of substrate, and OEDs are manufactured on transparent conductive film. Light is coming in from NML AR film, goes through the TCS, and then finally

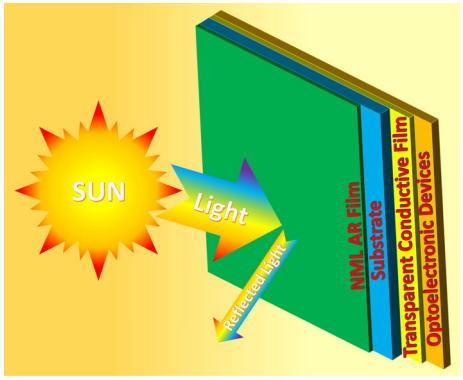

FIGURE 1. Diagram of TCS with NML AR film.

enters into the OEDs. In this article, our NML AR film is at the interface between substrate and air. This kind of NML AR films are easy to fabricate by physical vapor deposition on the existing TCSs, which can realize mass production in business without knowing the craftsmanship of transparent conductive film.

In the following sections, we will investigate the NML AR films on three kinds of substrates, which are glass, PEN, and PET. It is worth noting that the PEN and PET plastic is flexible, which can be used for flexible OEDs [28]–[31].

In TFO design, low and high index materials are necessary to achieve the desired optical target. The materials should have low chromatic dispersity and no absorption. In this study, the low index material is MgF_2, and the high index material is Ta_2O_5. Once the material is selected, the thickness of every layer of NML will determine the optimized result. Encouragingly, these thicknesses can be obtained by optical target optimization simulation of Essential Macleod or other commercial software.

Optical target optimization simulation requires the knowledge of optical parameters of the materials. The refractive index n and extinction coefficient k dependence on the wavelength λ (nm) for all the materials in this study can be obtained from the pioneer published works [32]–[34], as shown in Fig. 2. However, every different fabrication method with different condition will influence the optical parameters of material, and then influence the final designs. If researchers want to compare the experimental data with the theoretical results, they must obtain the optical property of every layer material in their experiment condition by ellipsometer.

Here we have ignored the magnetic effect, and the relative permeability of all above materials is assumed to be 1. However, there are two kinds of glass, which are white glass and electron-grade glass. In usual, the white glass is used for ITO glass, and the electron-grade glass is used for FTO glass. Optical properties of these two glasses are different. To simplify the problem, the substrate glasses in our following study are all white glass. Generally, the relative permittivity of air is 1.

TABLE 1. The detailed design of the NML AR film on glass.

ARB	Layer No.	Sub.	1	2	3	4	5	6	7	8	9	10	11	12	Inc.
~800nm	Mater.	Glass	Ta_2O_5	MgF_2	Ta_2O_5	MgF_2	Ta_2O_5	MgF_2							Air
	Thick. (nm)	1mm	18.17	32.00	40.87	28.33	27.38	102.49							
~1100nm	Mater.	Glass	Ta_2O_5	MgF_2	Ta_2O_5	MgF_2	Ta_2O_5	MgF_2	Ta_2O_5	MgF_2					Air
	Thick. (nm)	1mm	12.04	39.26	30.29	19.66	142.28	23.07	23.07	107.06					
~1500nm	Mater.	Glass	Ta_2O_5	MgF_2	Ta_2O_5	MgF_2	Ta_2O_5	MgF_2	Ta_2O_5	MgF_2	Ta_2O_5	MgF_2	Ta_2O_5	MgF_2	Air
	Thick. (nm)	1mm	10.13	46.06	24.63	35.01	37.72	15.74	158.41	12.81	37.96	38.43	18.04	121.47	

TABLE 2. The detailed design of the NML AR film on PEN.

ARB	Layer No.	Sub.	1	2	3	4	5	6	7	8	9	10	11	12	Inc.
~800nm	Mater.	PEN	Ta_2O_5	MgF_2	Ta_2O_5	MgF_2	Ta_2O_5	MgF_2							Air
	Thick. (nm)	1mm	21.22	12.43	94.25	12.97	22.00	90.14							
~1100nm	Mater.	PEN	Ta_2O_5	MgF_2	Ta_2O_5	MgF_2	Ta_2O_5	MgF_2	Ta_2O_5	MgF_2					Air
	Thick. (nm)	1mm	12.76	25.86	32.86	15.68	143.26	23.21	22.97	107.62					
~1500nm	Mater.	PEN	Ta_2O_5	MgF_2	Ta_2O_5	MgF_2	Ta_2O_5	MgF_2	Ta_2O_5	MgF_2	Ta_2O_5	MgF_2	Ta_2O_5	MgF_2	Air
	Thick. (nm)	1mm	10.60	30.04	28.62	28.44	41.00	13.16	164.40	13.25	37.95	38.91	18.07	122.61	

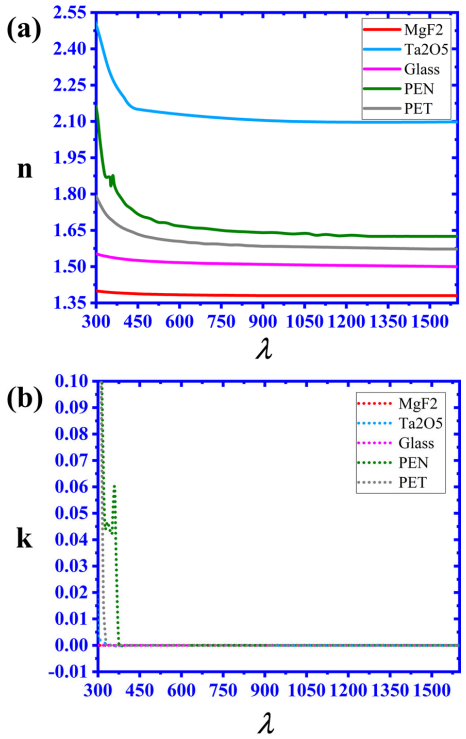

FIGURE 2. (a) Refractive index n dependence on the wavelength λ (nm) for the materials in this study; (b) extinction coefficient k dependence on the wavelength λ (nm) for the materials in this article.

III. DESIGNS OF THE NML AR FILMS

For different optoelectronic materials, there are different light absorbance bands. So in this section, based on substrates glass, PEN and PET, three kinds of AR bands (ARBs) are investigated, which are 350 nm ∼ 800 nm band, 350 nm ∼ 1100 nm band, and 350 nm ∼ 1500 nm band, respectively. The low and high index materials are MgF_2 and Ta_2O_5. The numbers of layers are 6, 8, and 12 for the three kinds of ARBs.

Tables 1-3 show the detailed designs of NML AR films with three kinds of AR bands for substrates glass, PEN and PET, respectively. The rows named Layer No. indicate the light comes from the incidence medium, crosses through the thin films, and then goes into the substrate medium. Inc. and Sub. are short for incidence medium and substrate medium, respectively. The following rows Mater. and Thick. (nm) are the material type and thickness of the corresponding Layer No.

The total thickness of ARBs ∼800nm, ∼1100nm and ∼1500nm for glass substrate are 249.24 nm, 396.73 nm and 556.41 nm, for PEN substrate are 253.01 nm, 384.22 nm and 547.05 nm, for PET substrate are 255.82 nm, 390.89 nm and 549.00 nm, respectively. It reflects that more layers are needed to widen ARB. The optical performance (transmittance and reflectance) of these NML AR films are shown in Figs. 3-5. Here we have ignored the transparent conductive films, such as ITO and FTO. Because the substrate thickness is 1 mm, and the transparent conductive films do not have influence on the AR films which are on the other side of the substrate.

For glass with the NML AR films in Fig. 3, the improvement of optical performance is obvious in corresponding ARB (∼800nm, ∼1100nm and ∼1500nm). For transmittance, as shown in sub-Figs. 3(a) and (b), the maximum transmittance of ARBs ∼800nm, ∼1100nm and ∼1500nm are about 95.5%, which are about 3.5% bigger than the no NML AR situation. For reflectance, as shown in sub-Figs. 3(c) and (d), the minimum reflectance of ARBs ∼800nm, ∼1100nm and ∼1500nm are about 4.5%, which are about 3.5% smaller than the no NML AR situation.

For PEN with the NML AR films in Fig. 4, the improvement of optical performance is obvious in corresponding ARB (∼800nm, ∼1100nm and ∼1500nm). For transmittance, as shown in sub-Figs. 4(a) and (b), the maximum transmittance of ARBs ∼800nm, ∼1100nm and ∼1500nm

TABLE 3. The detailed design of the NML AR film on PET.

ARB	Layer No.	Sub.	1	2	3	4	5	6	7	8	9	10	11	12	Inc.
~800nm	Mater.	PET	Ta_2O_5	MgF_2	Ta_2O_5	MgF_2	Ta_2O_5	MgF_2							Air
	Thick. (nm)	1mm	19.47	15.88	97.96	12.50	20.86	89.15							
~1100nm	Mater.	PET	Ta_2O_5	MgF_2	Ta_2O_5	MgF_2	Ta_2O_5	MgF_2	Ta_2O_5	MgF_2					Air
	Thick. (nm)	1mm	12.97	31.74	32.17	17.36	143.09	23.18	23.00	107.38					
~1500nm	Mater.	PET	Ta_2O_5	MgF_2	Ta_2O_5	MgF_2	Ta_2O_5	MgF_2	Ta_2O_5	MgF_2	Ta_2O_5	MgF_2	Ta_2O_5	MgF_2	Air
	Thick. (nm)	1mm	10.95	36.57	27.19	30.88	39.65	14.07	159.87	13.06	37.92	38.67	18.07	122.10	

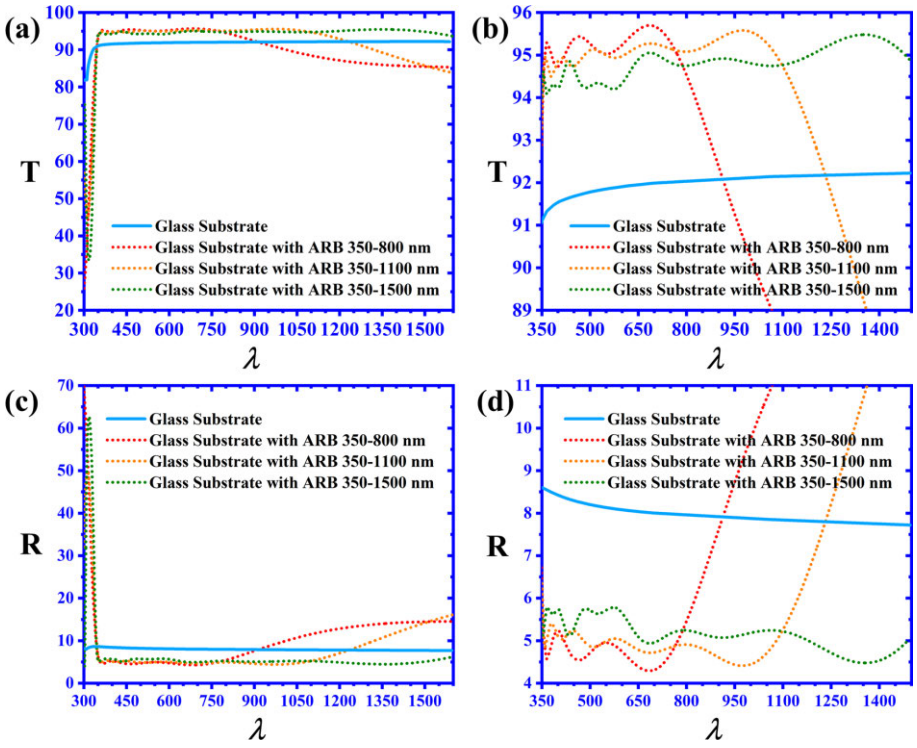

FIGURE 3. Transmittance (a, b) and reflectance (c, d) dependence on the wavelength λ (nm) of glass substrate with NML AR films of ARB 350-800nm (red dotted lines), with NML AR films of ARB 350-1100nm (yellow dotted lines), with NML AR films of ARB 350-1500nm (green dotted lines), and without any AR films (blue lines).

are about 94%, which are about 5.5% bigger than the no NML AR situation. For reflectance, as shown in sub-Figs. 4(c) and (d), the minimum reflectance of ARBs ∼800nm, ∼1100nm and ∼1500nm are about 5.5%, which are about 5% smaller than the no NML AR situation.

For PET with the NML AR films in Fig. 5, the improvement of optical performance is obvious in corresponding ARB (∼800nm, ∼1100nm and ∼1500nm). For transmittance, as shown in sub-Figs. 5(a) and (b), the maximum transmittance of ARBs ∼800nm, ∼1100nm and ∼1500nm are about 94.5%, which are about 4.5% bigger than the no NML AR situation. For reflectance, as shown in sub-Figs. 5(c) and (d), the minimum reflectance of ARBs ∼800nm, ∼1100nm and ∼1500nm are about 5%, which are about 4.5% smaller than the no NML AR situation.

Then we use the FEM (COMSOL Multiphysics) as a contrast of TFO to simulate the NML. In order to simulate the physical model, 3D geometry is selected, Radio Frequency (RF) module is chosen, and two Electromagnetic Waves (*emw*1 and *emw*2) Frequency Domains are used. The first physical domain *emw*1 is used to simulate the incident electromagnetic wave propagation in air, and the second physical domain *emw*2 is used to simulate AR NML situation with the electric field distribution of the first physical domain as the initial conditions. The incident electromagnetic wave follows the negative z direction, and the polarization of the electric field follow the x direction. Therefore, the electric field distribution of the first physical domain *emw*1.*Ex* represents the incident electromagnetic wave, and the electric field distribution of the second physical domain *emw*2.*Ex* represent the superposition of incident and reflected electromagnetic waves.

In COMSOL, the incidence electromagnetic field is TM (Transverse Magnetic) mode wave, as shown in Fig. 6(a).

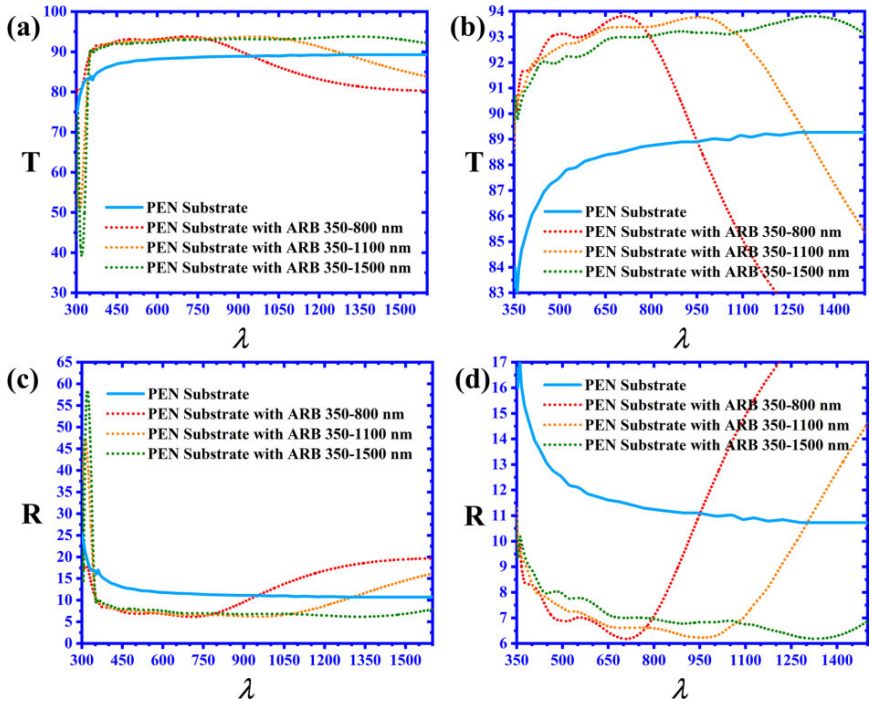

FIGURE 4. Transmittance (a, b) and reflectance (c, d) dependence on the wavelength λ (nm) of PEN substrate with NML AR films of ARB 350-800nm (red dotted lines), with NML AR films of ARB 350-1100nm (yellow dotted lines), with NML AR films of ARB 350-1500nm (green dotted lines), and without any AR films (blue lines).

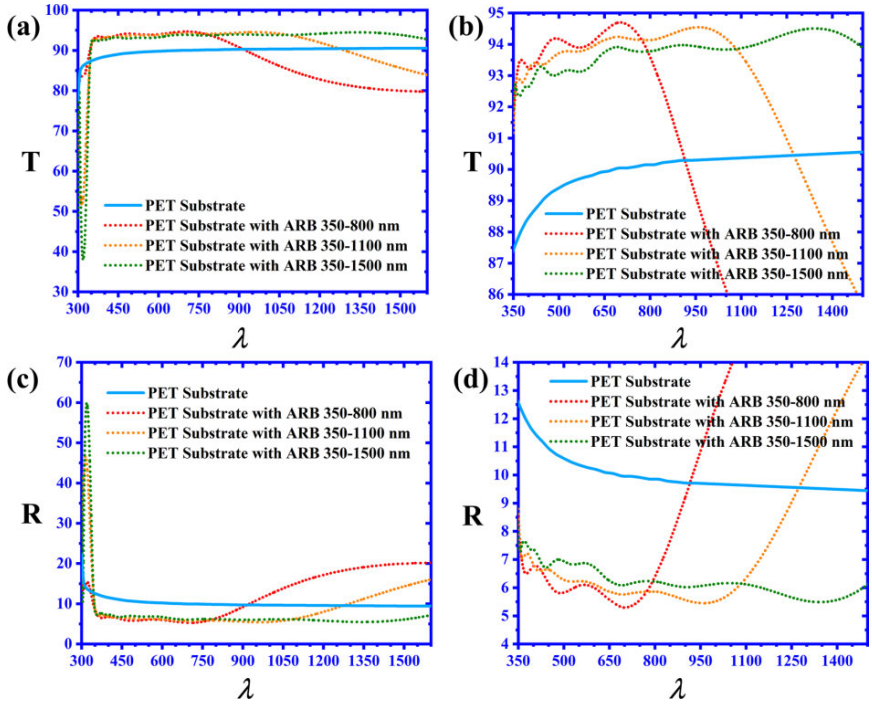

FIGURE 5. Transmittance (a, b) and reflectance (c, d) dependence on the wavelength λ (nm) of PET substrate with NML AR films of ARB 350-800nm (red dotted lines), with NML AR films of ARB 350-1100nm (yellow dotted lines), with NML AR films of ARB 350-1500nm (green dotted lines), and without any AR films (blue lines).

Ei and *Hi* are the electric field and magnetic field of the incident wave, while *Er* and *Hr* are the electric field and magnetic field of the reflected wave. Red arrows and yellow cross, respectively describe the directions of the electric field and magnetic field. Yellow cross means that the direction is perpendicular to the plane of the paper and inside it.

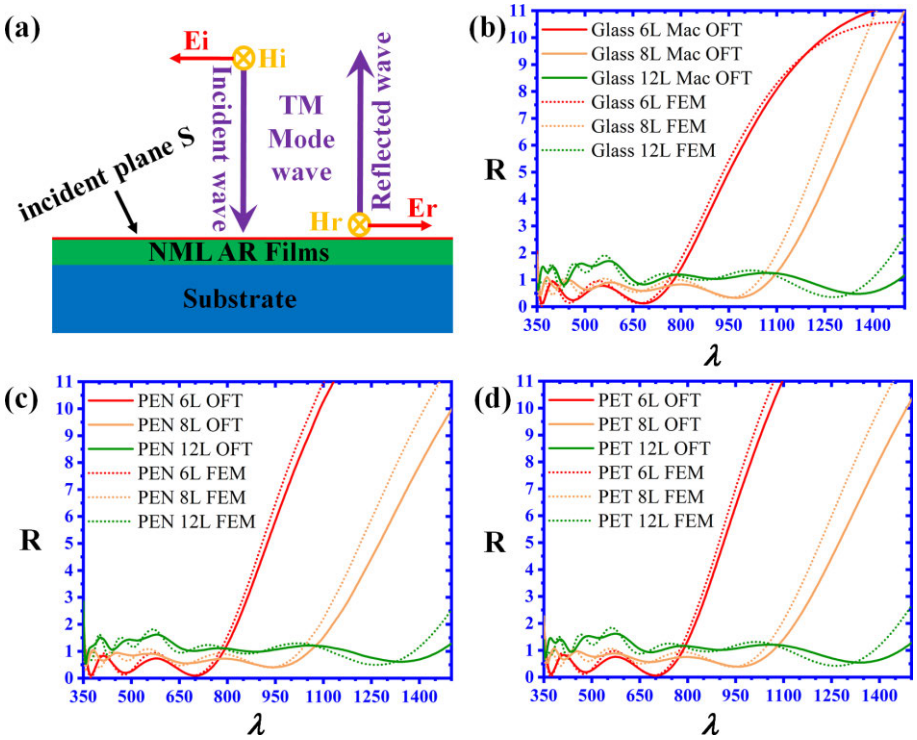

FIGURE 6. (a) The sketch of TM mode wave reflection; Reflectance dependence on the wavelength λ (nm) of glass (b) PEN (c) and PET (d) substrates with 6 (red lines) 8 (yellow lines) and 12 (green lines) layers NML AR films by TFO (solid lines) and FEM (dotted lines) methods.

TABLE 4. AARE of different substrates with different ARBs.

ARB \ Sub.	Glass	PEN	PET
AARE			
~800nm	**3.69%**	**6.15%**	**5.06%**
~1100nm	**3.46%**	**5.56%**	**4.62%**
~1500nm	**3.07%**	**5.02%**	**4.17%**

Consequently, $emw1.Ex = Ei$, and $emw2.Ex = Ei$ - Er. Integration can reduce the numerical noise error. Then the reflectance of the incident electric field ρ and energy flux R can be expressed as

$$\rho = \frac{\int_S emw1.Exds - \int_S emw2.Exds}{\int_S emw1.Exds}, \quad (1)$$

$$R = \rho \times \rho^*, \quad (2)$$

where S is the incident plane as shown in Fig. 6(a).

Because the thickness aberration of the hundreds nm films and 1mm substrate is too large, the mesh division in COMSOL is too close to affect the simulation speed. Therefore, the thickness of the substrate is ignored in the model simulation by COMSOL. So we are only thinking about the reflection on the front face of the substrate. In practice, the thickness of the substrate and end face both have effects on the reflectivity of the system. As shown in sub-Figs. 6(b) (c) and (d), the solid and dotted lines are the results from TFO and FEM, respectively. Sub-Figs. 6(b) (c) and (d) are reflectance dependence on the wavelength of glass (b) PEN (c) and PET (d) substrates with 6 (red lines) 8 (yellow lines) and 12 (green lines) layers NML AR films by TFO (solid lines) and FEM (dotted lines) methods. These results reflect that the two methods TFO and FEM agree well with each other. However, the obtained data for each of these curves by FEM takes about four hours, while the data by TFO only takes about a few seconds. It is worth noting that the difference between FTO and FEM results increases with the number of layers. That is because as the number of layers increases, the larger the mesh becomes, the greater the numerical error becomes.

Finally, we shall define a physical quantity AARE (shorted for average AR effect) to describe the average AR of different ARBs,

$$AARE = \frac{\int_{ARB} \frac{T_1 - T_2}{T_2} d\lambda}{ARB}, \quad (3)$$

where T_1 is the transmittance of NML AR substrate, and T_2 is the transmittance of none AR substrate.

Combining Eq. (3) with the data in Figs. (3)-(5), we can get the AARE of different substrates with different ARBs, as shown in Table 4. Finally, AAREs are about 3.69%, 3.46% and 3.07% on glass substrate, about 6.15%, 5.56% and 5.02% on PEN substrate, and about 5.06%, 4.62% and 4.17% on PET substrate, for AR bands (ARBs) 350~800 nm, 350~1100 nm and 350~1500 nm, respectively.

IV. CONCLUSION

We have theoretically investigated the AR films based on NML of MgF_2 and Ta_2O_5 on three kinds of substrates (glass, PEN and PET) for three kinds of ARBs (350∼800 nm, 350∼1100 nm, and 350∼1500 nm). This kind of low and high index dielectric NML structures have the advantages of low-cost and flexible. Such NML AR films can be used to improve the reflectance of air and substrate interface for TCS. The present method, i.e. using TFO to design NML AR films, will help to guide development of many kinds of OEDs.

ACKNOWLEDGMENT

(Dong Wang, Rui Zhou, and Yinghui Wu contributed equally to this work.)

REFERENCES

[1] D. Wang, J. Huang, Y. Lei, W. Fu, Y. Wang, P. Deng, H. Cai, and J. Liu, "Transparent conductive films based on quantum tunneling," *Opt. Express*, vol. 27, no. 10, pp. 14344–14352, 2019.

[2] B. M. Sa'ad, S. K. A. Rahim, T. Peter, M. S. B. A. Rani, S. F. Ausordin, D. N. A. Zaidel, and C. Krishnan, "Transparent branch-line coupler using micro-metal mesh conductive film," *IEEE Microw. Wireless Compon. Lett.*, vol. 24, no. 12, pp. 857–859, Dec. 2014.

[3] J.-K. Sheu, M.-L. Lee, Y. S. Lu, and K. W. Shu, "Ga-doped ZnO transparent conductive oxide films applied to GaN-based light-emitting diodes for improving light extraction efficiency," *IEEE J. Quantum Electron.*, vol. 44, no. 12, pp. 1211–1218, Dec. 2008.

[4] Z. Wang, P. Yi, L. Peng, X. Lai, and J. Ni, "Continuous fabrication of highly conductive and transparent ag mesh electrodes for flexible electronics," *IEEE Trans. Nanotechnol.*, vol. 16, no. 4, pp. 687–694, Jul. 2017.

[5] H. Lu, J. Luo, Y. Liu, Y. Zhong, J. Wang, and Y. Zhang, "Highly performance flexible polymer solar cells by flipping the bilayer film of ag nanowires and polyvinyl alcohol on polyethylene terephthalate as transparent conductive electrodes," *IEEE J. Photovolt.*, vol. 9, no. 3, pp. 710–714, May 2019.

[6] N. Ye, T. Liang, L. Zhan, Y. Kong, S. Xie, X. Ma, H. Chen, H. Su, and M. Xu, "High-performance bendable organic solar cells with silver nanowire-graphene hybrid electrode," *IEEE J. Photovolt.*, vol. 9, no. 1, pp. 214–219, Jan. 2019.

[7] K. Ellmer, "Past achievements and future challenges in the development of optically transparent electrodes," *Nature Photon.*, vol. 6, no. 12, pp. 809–816, 2012.

[8] J. Gao, K. Kempa, M. Giersig, E. M. Akinoglu, B. Han, and R. Li, "Physics of transparent conductors," *Adv. Phys.*, vol. 65, no. 6, pp. 553–617, 2016.

[9] H. Lee, Z. Baghdasaryan, B. Friedman, and K. Lee, "Electrical defect imaging of ITO coated glass by optical microscope with microwave heating," *IEEE Access*, vol. 7, pp. 42201–42209, 2019.

[10] K.-H. Tsui, Q. Lin, H. Chou, Q. Zhang, H. Fu, P. Qi, and Z. Fan, "Low-cost, flexible, and self-cleaning 3D nanocone anti-reflection films for high-efficiency photovoltaics," *Adv. Mater.*, vol. 26, no. 18, pp. 2805–2815, 2014.

[11] C. Zhang, Y. Song, M. Wang, M. Yin, X. Zhu, L. Tian, H. Wang, X. Chen, Z. Fan, L. Lu, and D. Li, "Efficient and flexible thin film amorphous silicon solar cells on nanotextured polymer substrate using sol–gel based nanoimprinting method," *Adv. Funct. Mater.*, vol. 27, no. 13, pp. 1604720–1604727, 2017.

[12] Y. Yao, K.-T. Lee, X. Sheng, N. A. Batara, N. Hong, J. He, L. Xu, M. M. Hussain, H. A. Atwater, N. S. Lewis, R. G. Nuzzo, and J. A. Rogers, "Porous nanomaterials for ultrabroadband omnidirectional anti-reflection surfaces with applications in high concentration photovoltaics," *Adv. Energy Mater.*, vol. 7, no. 7, pp. 1601992–1602000, 2017.

[13] R. R. Lunt and V. Bulovic, "Transparent, near-infrared organic photovoltaic solar cells for window and energy-scavenging applications," *Appl. Phys. Lett.*, vol. 98, no. 11, Mar. 2011, Art. no. 113305.

[14] R. Betancur, P. Romero-Gomez, A. Martinez-Otero, X. Elias, M. Maymó, and J. Martorell, "Transparent polymer solar cells employing a layered light-trapping architecture," *Nature Photon.*, vol. 7, pp. 995–1000, Dec. 2013.

[15] F. Pastorelli, P. Romero-Gomez, R. Betancur, A. Martinez-Otero, P. Mantilla-Perez, N. Bonod, and J. Martorell, "Enhanced light harvesting in semitransparent organic solar cells using an optical metal cavity configuration," *Adv. Energy Mater.*, vol. 5, no. 2, Jan. 2015, Art. no. 1400614.

[16] A. H. Safavi-Naeini, J. T. Hill, S. Meenehan, J. Chan, S. Gröblacher, and O. Painter, "Two-dimensional phononic-photonic band gap optomechanical crystal cavity," *Phys. Rev. Lett.*, vol. 112, no. 15, Apr. 2014, Art. no. 153603.

[17] S. Chattopadhyay, Y. F. Huang, Y. J. Jen, A. Ganguly, K. H. Chen, and L. C. Chen, "Anti-reflecting and photonic nanostructures," *Mater. Sci. Eng., R, Rep.*, vol. 69, nos. 1–3, pp. 1–35, Jun. 2010.

[18] D. Wang, J. Song, J. Xian, Y. Tian, L. Chen, S. Ye, H. Niu, and J. Qu, "Characteristic analysis of broadband plasmonic emitting devices based on transformation optics," *Opt. Express*, vol. 23, no. 12, pp. 16109–16121, 2015.

[19] D. Wang, J. Song, M. Xiong, G. Wang, X. Peng, and J. Qu, "Modified method for computing the optical force of the plasmonics nanoparticle from the Maxwell stress tensor," *J. Opt. Soc. Amer. B, Opt. Phys.*, vol. 34, no. 1, pp. 178–182, 2017.

[20] H. A. Macleod, *Thin-Film Optical Filters*, 3rd ed. London, U.K.: Institute of Physics, 2001.

[21] C. C. Lee and Y.-J. Chen, "Multilayer coatings monitoring using admittance diagram," *Opt. Express*, vol. 16, no. 9, pp. 6119–6124, 2008.

[22] Q.-Y. Cai, Y.-X. Zheng, D.-X. Zhang, W.-J. Lu, R.-J. Zhang, W. Lin, H.-B. Zhao, and L.-Y. Chen, "Application of image spectrometer to *in situ* infrared broadband optical monitoring for thin film deposition," *Opt. Express*, vol. 19, no. 14, pp. 12969–12977, 2011.

[23] K. Wu, C.-C. Lee, and T.-L. Ni, "Advanced broadband monitoring for thin film deposition through equivalent optical admittance loci observation," *Opt. Express*, vol. 20, no. 4, pp. 3883–3889, 2012.

[24] Q. Y. Cai, H.-H. Luo, Y.-X. Zheng, and D.-Q. Liu, "Design of no-polarizing cut-off filters based on dielectric-metal-dielectric stacks," *Opt. Express*, vol. 21, no. 16, pp. 19163–19172, 2013.

[25] D. Wang, Y. Wang, J. Huang, W. Fu, Y. Lei, P. Deng, H. Cai, and J. Liu, "Low-cost and flexible anti-reflection films constructed from nano multi-layers of TiO_2 and SiO_2 for perovskite solar cells," *IEEE Access*, vol. 7, pp. 176394–176403, 2019.

[26] H. Guan, P. Han, Y. Yang, Y. Li, X. Zhang, and W. Zhang, "Omni-directional mirror for visible light based on one-dimensional photonic crystal," *Chin. Opt. Lett.*, vol. 9, no. 7, 2011, Art. no. 071603.

[27] L. E. Puente-Díaz, V. Castillo-Gallardo, G. P. Ortiz, J. S. Pérez-Huerta, H. Pérez-Aguilar, V. Agarwal, and W. L. Mochán, "Stable calculation of optical properties of large non-periodic dissipative multilayered systems," *Superlattices Microstructures*, vol. 145, Sep. 2020, Art. no. 106629.

[28] T. Sannicolo, M. Lagrange, A. Cabos, C. Celle, J.-P. Simonato, and D. Bellet, "Metallic nanowire-based transparent electrodes for next generation flexible devices: A review," *Small*, vol. 12, no. 44, pp. 6052–6075, Nov. 2016.

[29] O. Ostroverkhova, "Organic optoelectronic materials: Mechanisms and applications," *Chem. Rev.*, vol. 116, no. 22, pp. 13279–13412, Nov. 2016.

[30] J. Feng, X. Zhu, Z. Yang, X. Zhang, J. Niu, Z. Wang, S. Zuo, S. Priya, S. Liu, and D. Yang, "Record efficiency stable flexible perovskite solar cell using effective additive assistant strategy," *Adv. Mater.*, vol. 30, no. 35, Aug. 2018, Art. no. 1801418.

[31] M. Pandey, Z. Wang, G. Kapil, A. K. Baranwal, D. Hirotani, K. Hamada, and S. Hayase, "Dependence of ITO-coated flexible substrates in the performance and bending durability of perovskite solar cells," *Adv. Eng. Mater.*, vol. 21, no. 8, Aug. 2019, Art. no. 1900288.

[32] N. Hong, R. A. Synowicki, and J. N. Hilfiker, "Mueller matrix characterization of flexible plastic substrates," *Appl. Surf. Sci.*, vol. 421, pp. 518–528, Nov. 2017.

[33] P. Prepelita, M. Filipescu, I. Stavarache, F. Garoi, and D. Craciun, "Transparent thin films of indium tin oxide: Morphology–optical investigations, inter dependence analyzes," *Appl. Surf. Sci.*, vol. 424, pp. 368–373, Dec. 2017.

[34] I. L. Elviyanti, H. Purwanto, and Kusumandari, "Optical simulation of surface textured TCO using FDTD method," *IOP Conf. Ser., Mater. Sci. Eng.*, vol. 107, Feb. 2016, Art. no. 012024.

DONG WANG received the B.S. degree in optical information science and technology and the Ph.D. degree in optical engineering from the Huazhong University of Science and Technology, China, in 2009 and 2014, respectively. He is currently a Postdoctoral Researcher with the College of Physics and Optoelectronic Engineering, Shenzhen University, China. His research interests include optical films, quantum optics, transformation optics, and nano-structure optics.

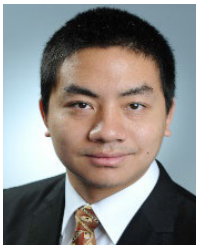

RUI ZHOU received the B.Sc. degree in automobile engineering from Tongji University, in 2010, and the M.Sc. degree in automobile engineering from the Technical University of Braunschweig, in 2014. He is currently working as a Research and Development Director with Waytous Inc., China. He has served as a Software Engineer and a Test Engineer for Daimler AG., Stuttgart and Ford-Werke GmbH, Cologne. His research interests include autonomous vehicle, test area for intelligent-connected vehicle, functional safety, and optical films.

YINGHUI WU is currently a Postdoctoral Researcher with the College of Physics and Optoelectronic Engineering, Shenzhen University, China. His research interests include related to design of ultrafast solar cell and optical films

HOUZHI CAI received the B.S. degree in optical information science and technology from the Huazhong University of Science and Technology, China, in 2004, and the M.S. and Ph.D. degrees in optical engineering from Shenzhen University, China, in 2007 and 2010, respectively. He is currently an Associate Professor with the College of Physics and Optoelectronic Engineering, Shenzhen University. His research interests include design and characterization of ultrafast sensors with sub-nanosecond temporal resolution and optical films.

YUEQIANG ZHANG is currently an Associate Professor with the College of Physics and Optoelectronic Engineering, Shenzhen University, China. His research interests include machine vision, artificial intelligence, and optical measurement.